Modelling the fracture behavior of thermal barrier coatings containing healing particles

Jayaprakash Krishnasamy[a,*], Sathiskumar A. Ponnusami[a,b], Sergio Turteltaub[a], Sybrand van der Zwaag[a]

[a] *Faculty of Aerospace Engineering, Delft University of Technology, Kluyverweg 1, 2629 HS Delft, The Netherlands*

[b] *Solid Mechanics and Materials Engineering, Department of Engineering Science, University of Oxford, Parks Road, OX1 3PJ Oxford, United Kingdom*

Abstract

The performance of a self-healing Thermal Barrier Coating (TBC) containing dispersed healing particles depends crucially on the mismatch in thermomechanical properties between the healing particles and the TBC matrix. The present work systematically investigates this phenomenon based on numerical simulations using cohesive element-based finite element analysis. The effect of the mismatch in Coefficient of Thermal Expansion (CTE) and fracture strength between the healing particles and the matrix on the fracture characteristics is quantified in detail. Unit cell-based analyses are conducted on a representative self-healing TBC system under a thermal loading step typically experienced by TBC systems in jet turbines. Two different simulation setups are considered within the TBC unit cell namely (i) a single pair of healing particles and (ii) a randomly distributed array of healing particles. The results of the simulations are reported in terms of the fracture pattern, crack initiation temperature and crack length for various CTE mismatch ratios. Correlations are established between the results obtained from the two simulation setups essentially revealing the effect of spatial distribution and proximity of healing particles on the fracture pattern. The results obtained from the analyses can be utilised to achieve a robust design of a self-healing TBC system.

Keywords: Thermal barrier coatings, cohesive elements, healing particles, thermal mismatch, fracture mechanics

1. Introduction

Thermal Barrier Coating (TBC) systems are protective layers applied to critical structural components of jet engines operating at high-temperature. A typical TBC system

*Corresponding author

Email addresses: J.Krishnasamy-1@tudelft.nl (Jayaprakash Krishnasamy), sathis.ponnusami@eng.ox.ac.uk (Sathiskumar A. Ponnusami), S.R.Turteltaub@tudelft.nl (Sergio Turteltaub), S.vanderZwaag@tudelft.nl (Sybrand van der Zwaag)

consists of three different layers, (i) a Top Coat (TC), which directly faces the hot gases in the engine (ii) a Thermally Grown Oxide layer (TGO) and (iii) a Bond Coat (BC) layer which is connected to the actual turbine blades. The TC layer is a ceramic layer usually consisting of Yttria Stabilized Zirconia (YSZ). It provides thermal insulation to the underlying components because of its low thermal conductivity. The BC layer is an intermediate metallic layer often made of NiCoCrAlY alloy. It acts as a bonding layer connecting the TC and the substrate and also provides oxidation resistance to the substrate by acting as a sacrificial layer. The TGO layer is a relatively thin α alumina (Al_2O_3) layer formed due to the oxidation of the aluminium phase in the BC at high temperatures. The coating system undergoes a thermal cycle during each start and stops as the turbine's temperature increases from ambient to operating temperature and subsequently decreases back to the ambient temperature. During each thermal cycle, the layers of the TBC system expand and shrink unequally due to a mismatch in coefficients of thermal expansion (CTE) of the TBC layers as illustrated in Fig. 1.a. The resulting thermal stresses cause nucleation and growth of micro-cracks in the TBC system [1, 2]. In addition, cracking also occurs due to the thickening of the TGO layer as the oxidation of the metallic bond coating generates more alumina, see Fig. 1.a and b. After several hundreds of thermal cycles, the micro-cracks eventually coalesce, forming a relatively large crack originally more or less parallel to the TBC-substrate interface. As large cracks deflect towards the free surface via local imperfections, the TBC separates from the substrate, which is known as spallation, as illustrated in Fig. 1.b. As a consequence, large portions of the TC separate, which may lead to direct exposure of the critical engine components to the high-temperature gases, ultimately resulting in a catastrophic failure of the entire turbine.

Several efforts have been made to increase the lifetime of the TBC system, mainly in the directions of varying the deposition process and coating compositions in order to delay the initiation of micro-cracks [3, 4, 5]. Incorporating self-healing mechanisms in TBC systems is a novel approach to improve the lifetime of these coatings [6, 7, 8, 9, 10]. The principle of the self-healing mechanism in a TBC system is demonstrated in Fig. 1.c [7]. A solid self-healing agent is encapsulated and embedded within the TBC topcoat layer during the coating process. When the crack induced by thermal cycling reaches the microcapsule, the capsule breaks and the oxidised self-healing agent flows into the crack, where it can further react with the matrix material and heal the crack. The best studied concept of the self-healing TBC is based on alumina coated Mo-Si particles embedded in the TC layer close to the TC/BC coat interface where the micro-cracks are likely to initiate. Upon cracking in the TBC, the micro-cracks interact with the healing particles, resulting in fracture of the particles. Subsequently, the healing agent within the particles oxidises and diffuses into the crack to form a glassy phase which in turn reacts with the surrounding matrix to form a load-bearing crystalline ceramic (zircon). The resulting healing of the micro-cracks delays the formation of a macro-crack by preventing crack coalescence which, in turn, extends the life time of the TBC system. Further details of the above-discussed self-healing TBC system such as detailed description of the healing mechanism, type of healing particle, fabrication routes and associated challenges can be found in the following works [11, 6, 7, 8, 12, 13].

Numerous computational studies have been conducted to investigate the failure mecha-

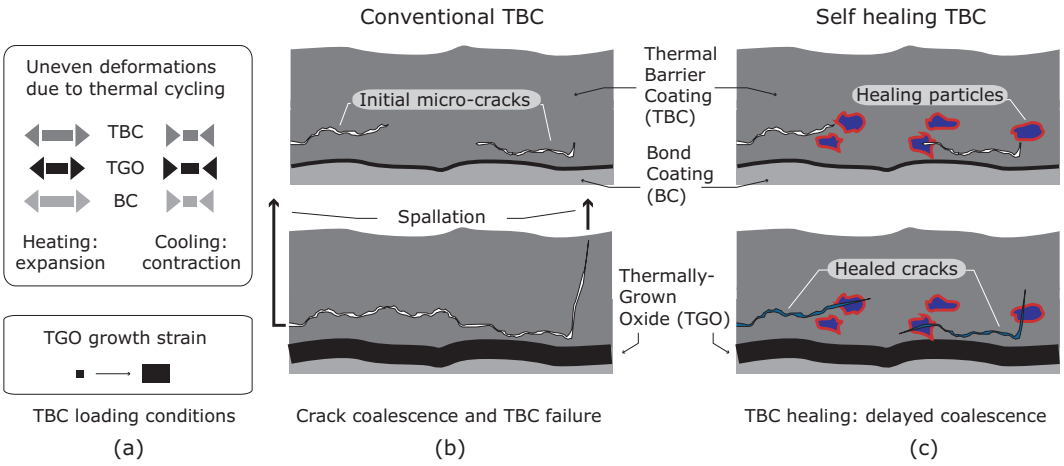

Figure 1: Schematic of TBC failure mechanisms and principle of a self-healing TBC system.

nisms in the TBC system. In the context of fracture analysis in TBC systems, different approaches have been used, including, classical fracture mechanics-based methods (e.g. VCCT, energy release rate) [14, 15], cohesive zone element based methods [16, 17] and the extended finite element method (XFEM) [18, 19]. Classical fracture mechanics approaches are suitable for crack propagation studies, whereas cohesive element-based approach enables modelling of crack initiation as well as crack propagation. XFEM is an enriched version of the classical finite element method which embeds discontinuities in the shape functions of a classical 2-D or 3-D finite element. This method serves as a tool to represent initial and evolving crack geometry independent of the finite element mesh and the crack evolution can be modelled either using classical fracture mechanics parameters or cohesive traction-separation laws. One of the current shortcomings of XFEM is its limited capability in dealing with multiple cracking and coalescence, which are crucial in the current study. Cohesive elements were utilised successfully for such multiple cracking and coalescence problems albeit with higher computational costs to achieve 'mesh-independent' solutions. A detailed review on various modelling methodologies and failure mechanisms in TBC systems addressed through computational modelling can be found in [20]. A second review on the influence of modelling choices in terms of interface morphology, boundary conditions, dimensionality and material models on the TBC response is presented in [21]. They provided guidelines and strategies for effectively modelling the stress evolution and the crack propagation in TBC systems. All the investigations in the literature have contributed to a detailed understanding of the failure mechanisms in TBC systems.

From the perspective of modelling the behavior of a self-healing TBC system, additional aspects need to be accounted for in the analysis as compared to the conventional TBC systems. Specifically, the effect of the presence of healing particles on the TBC fracture behaviour has to be analysed from two different perspectives. Firstly, to successfully trigger healing mechanism, the microcracks initiated in the TBC have to interact with healing particles leading to the opening of the particles for healing activation. This, in turn, depends on the geometric and the material properties of the healing particles in relation to the TBC

layers. Secondly, it is essential to study how the healing particles influence the thermomechanical behaviour of the self-healing TBC in comparison with the baseline TBC without healing particles, in other words, introducing healing particles should not significantly deteriorate the mechanical integrity of the original TBC system. Several modelling studies have been conducted in the literature to address the above two aspects [22, 23, 24, 25, 26, 27]. For instance, the influence of mechanical properties of the healing particles on the fracture mechanism in a self-healing material have been analysed in detail in [28, 27]. In [22], crack propagation studies were conducted in an idealized healing capsule(s)-matrix system and the effects of geometric and material parameters were analysed using cohesive and extended finite element method (XFEM). Within the context of self-healing TBC systems, few modelling studies have addressed the effect of the healing particles on the TBC properties and the thermomechanical response [29, 30]. The effect of the healing particles on the fracture mechanisms and the mechanical properties of a particulate composite representing a self-healing TBC microstructure were studied using cohesive element-based finite element analysis in [31, 32, 33]. However, one critical aspect that has not been analysed in detail pertains to the mismatch in thermo-elastic properties coupled to a mismatch in fracture properties.

In order to design a self-healing TBC system with dispersed healing particles, an important issue that needs detailed understanding is the effect of mismatch in CTE between the particles and the TBC layers, in addition to the elastic and fracture property mismatch. An ideal self-healing TBC should have healing particles with similar CTE in relation to the surrounding TC layer. Such a combination would prevent generation of additional thermal stresses in the TBC which would otherwise lead to microcrack formation. On a different context, specific prerequisites on the mechanical properties of the healing particles and the particle/matrix interface are necessary for a successful activation of the healing mechanism [28]. With this motivation, a detailed finite element analysis is conducted to quantify the effect of mismatch in thermomechanical properties on the fracture evolution in the self-healing TBC system. The effect of CTE mismatch is investigated in detail using two simulation setups, one with a TBC containing two healing particles and the other with a TBC consisting of a randomly distributed array of particles. Further, the effects of the relative strength of the particle and the interface with respect to the TC layer are analysed using the finite element simulations on the multiple particles setup. The present work is connected to the optimal design of self healing TBCs from two distinct aspects: (1) It serves as an analysis tool to decide the best combination of thermomechanical properties of the healing particles and the matrix to achieve a robust self-healing system and (2) It allows to choose the best spatial arrangement of healing particles to control the crack and healing patterns.

2. Finite element model of TBC

2.1. Model geometry

A 2D multiscale approach is adopted for the finite element analysis of fracture evolution in a self-healing TBC system. The system considered is composed of two different layers of

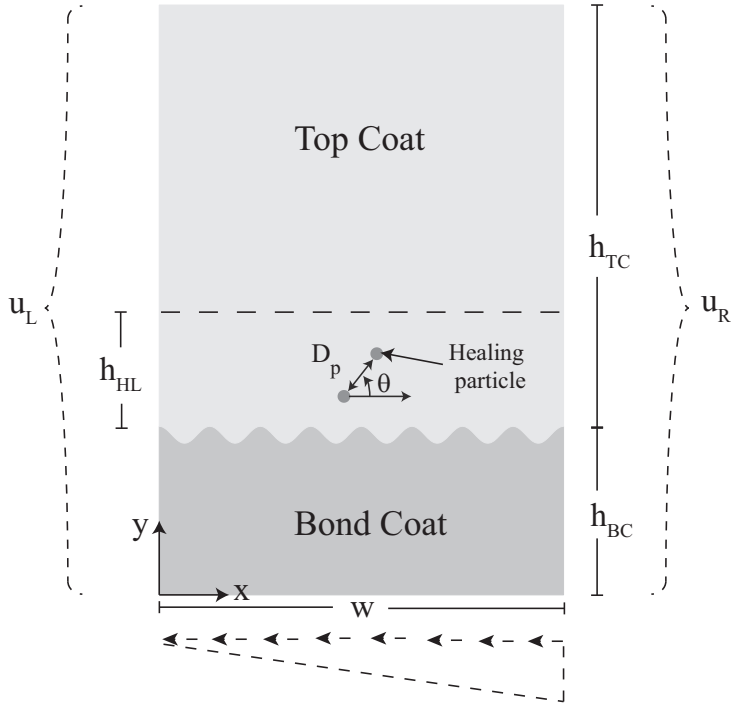

Figure 2: Finite Element Geometry showing two healing particles.

the TBC system, namely the TC and the BC. The TBC unit cell is periodic in the horizontal direction, while in the vertical direction, the layers are modelled with their respective thicknesses. The interface between the TC and the TGO layers is modelled as an idealised sinusoidal curve [34], whose wavelength and amplitude are assigned values of 60 μm and 10 μm respectively. These values are representative of a typical interface morphology in the air plasma sprayed TBC systems [35]. The thickness of the TC and the BC layers are taken as $h_{TC} = 500$ μm and $h_{BC} = 200$ μm respectively. The TGO layer is usually a thin layer whose thickness increases during operation (as a function of thermal cycles/time). The evolution of the TGO thickness is not modelled since only a single thermal cycle is analysed during which the growth of the TGO is negligible. Since the objective is to investigate the role of the healing particles and the property mismatch on the cracking pattern the TGO layer is not considered in the present analysis. Correspondingly, the loading condition considered in this work represents a typical (single) thermal cycle of an as-deposited TBC system.

As discussed earlier, the healing particles made of $MoSi_2$ are dispersed in the TC layer closer to the TGO layer representing the self-healing TBC architecture reported in [6]. Dispersing healing particles close to the TGO layer would be an effective approach as the microcracks are expected in such regions [8]. Fig.2 shows one of the configurations considered in the study in which a pair of healing particles is dispersed in the TC layer, whose location is characterised by the interparticle distance (D_p) and the orientation (θ). The modelling approach is then extended to a system containing randomly distributed healing particles, whose details will be discussed in corresponding sections. The unit cell is meshed with two-

dimensional three-noded plane strain triangular elements using the open source software GMSH [36]. To model fracture, cohesive elements are embedded throughout the finite element mesh regions in the unit cell using a Matlab script. Finite element analysis is carried out using the commercial software Abaqus. The insertion of cohesive elements throughout the finite element mesh enables arbitrary crack initiation and propagation, an important requirement in a complex system such as a TBC containing healing particles. One important consideration while using cohesive elements everywhere is the mesh dependency effect. A random and sufficiently fine mesh is a prerequisite in order to obtain a converged fracture pattern [28]. The element size is also chosen carefully to fulfill the requirements of properly resolving the cohesive zone. The region where the cracks are likely to nucleate and grow is finely meshed with an element size of 1 μm. The remaining regions of the TBC unit cell are meshed with an element size of 2 μm. The domain convergence analysis is carried out to find an appropriate width (W) of the periodic unit cell based on the convergence of critical temperature (onset of unstable crack growth). For W = 480 μm and W = 960 μm the percentage error in critical temperature is around 5 %. Hence, W of 480 μm is chosen for modelling the periodic unit cell. The finite element model is two-dimensional which poses limitations on the scope as actual three-dimensionality of the TBC microstructure is lost. However, a two-dimensional approach can be used effectively to unveil the failure mechanisms in TBC as it captures the most of the important features of the microstructure. Further, considering the size of the unit cell and the level of microstructural details of the considered self-healing TBC system, a three-dimensional analysis is not feasible to investigate in detail the effect of geometric and material parameters on fracture evolution.

2.2. Loading and boundary conditions

The substrate of the TBC, whose dimension is orders of magnitude larger than the individual layers of the TBC, is not modelled explicitly. Rather, its effect is accounted for through enforcement of boundary conditions derived using the thermal deformations induced by the substrate during a thermal cycle [37]. Due to its dimensions, the thermal deformation of the substrate can be assumed to be unaffected by the TBC layer. With this assumption, the induced thermal deformations can be obtained, and these displacements are then enforced as periodic conditions in the TBC unit cell as given in Eq.(1) for the left (L) and right (R) edges of the unit cell,i.e.,

$$\begin{aligned} u_x^R - u_x^L &= (1+\nu_s)\alpha_s \Delta T W, \\ u_y^R - u_y^L &= 0, \end{aligned} \tag{1}$$

where ν_s and α_s correspond to Poisson's ratio and the coefficient of thermal expansion, respectively and the subscript s refers to the substrate. The bottom (B) edge of the unit cell is subjected to the following displacement field:

$$\begin{aligned} u_x^B &= (1+\nu_s)\alpha_s \Delta T x, \\ u_y^B &= 0, \end{aligned} \tag{2}$$

whereas the top surface of the TBC is modelled as traction-free.

A typical thermal cycle that a TBC undergoes during operation consists of an ascending branch where the temperature rises more or less linearly from room temperature to operating high temperature, followed by a constant temperature operating period and finally cooling down phase back to the room temperature. In the literature, it is assumed that the TBC is stress-free at operating temperature (1100^oC) as the coating is deposited at around similar temperature range [1, 38]. The third phase of the cycle corresponds to a cooling phase in which thermal mismatch stresses develop and cracks are expected to initiate. Hence, this cooling down phase of the cycle is considered as the loading case whereby the temperature in the TBC model is gradually decreased from 1100^oC to 30^oC. As the crack formation is based on an quasi-static analysis, the cooling rate does not play a role and the system is assumed to be in thermal equilibrium at all times.

2.3. Constitutive models and material properties

The behaviour of the TBC system is strongly governed by the mismatch in the thermo-mechanical properties of the individual layers of the TBC system. The constitutive material behaviour of the different layers is assumed to be linear elastic and isotropic. A bilinear traction-separation law is used as the constitutive relation for the cohesive elements with different cohesive properties assigned for each layer and the interface in the TBC system. With cohesive elements embedded everywhere, another important aspect to be addressed is the way the periodic boundary conditions are applied on the edges where at a given nodal location, there is usually more than one node. Appropriate pairs of nodes are identified on the left and the right edges, which upon the enforcement of the boundary conditions does not prevent any crack to pass through and open the edges when required by the process, i.e., the artificial arrest of cracking in the edges is prevented.

The Youngs modulus E, Poisson's ratio ν and coefficient of thermal expansion α for the distinct phases are summarised in Table 1. The elastic and thermal properties of the TC are chosen similar to the values reported in [39, 40]. The elastic properties and the thermal expansion coefficient of the BC are chosen close to the values given in [41]. The stiffness of the healing particles is assumed to be 3 times larger than the stiffness of the TC [31]. The mode I (normal) fracture strength σ^n and the mode I fracture energy G^{IC} of the TC, the BC and the healing particles are considered in accordance with [42, 43, 44], where the values of the fracture energies reported in Table 1 have been calculated from the fracture toughness K^{IC} under plane strain and small plastic zone assumptions, i.e.,

$$G^{IC} = \frac{(K^{IC})^2(1-\nu)}{E}. \tag{3}$$

The ratio of the shear strength to the normal strength for the TC is taken as $\gamma_{TC} = 4$. This value is in-line with the experimental observations that the ceramic TBC fails in tension (Mode I) rather than in shear (Mode II). For simplicity, the same value of γ_{TC} is also used for the ratio between the mode I and mode II fracture toughness. For the BC, which is a metallic layer, the ratio is taken as $\gamma_{BC} = 1$. As indicated in Table 1 distinct values for the properties of the healing particles are considered. The BC/TC interface is chosen to have the fracture properties of the BC. Unless explicitly specified, the normal fracture strength,

Layers	E (GPa)	ν	α (10^{-6} 1/°C)	σ^n (MPa)	G^{IC} (N/mm)	γ
Top coat	80	0.15	12.5	100	0.002	4
Bond coat	130	0.3	14.5	500	0.3	1
Healing particle	250	0.22	varied	varied	0.02	varied
Substrate	200	0.28	16	-	-	-

Table 1: Elastic and fracture material parameters of the TBC components.

(σ^n_P, $\sigma^n_{i_{P/TC}}$) and the mixed-mode strength ratio, (γ_P, $\gamma_{i_{P/TC}}$) of the healing particles and the healing particle/TC interface are assumed to be equal and are taken as 300 MPa and 4, respectively. The influence of the fracture properties of the particles and the interface are analysed separately in Sec. 3.3 and Sec. 3.4 by considering different values for the strength of the particle and the interface.

3. Results and discussions

Three thermomechanical material parameters are considered for the analyses, namely (a) the CTE mismatch between the healing particles and the TC matrix, (b) the relative strength of the healing particle with respect to the TC layer and (c) the strength of the interface between the TC matrix and the particle. Finite element analyses on the TBC unit cell with boundary and loading conditions as described in Sec. 2.2 are conducted for a range of the above three material parameters, and the results are summarised in terms of the fracture pattern and the crack evolution kinetics in the TBC layers in the following sections.

In the context of cohesive element approach, crack initiation occurs when the traction in the element exceeds the material strength, and the crack is said to be fully formed when the amount of energy per unit area dissipated in the element is equal to the fracture energy of the material phase. In a system containing different phases with significantly different fracture energy values between the phases, it is not straightforward to define a failed state of the element in the different material phases. For instance, in the present situation, the fracture energy of the TC layer is 10 times lower than that of the healing particles. This would mean that the complete failure of a particle cohesive element is reached only when the energy dissipated in the crack opening is 10 times as compared to that of the complete failure of the TC cohesive element. Nonetheless, in both cases, the cohesive crack initiation would have started already. Thus, in order to have a useful interpretation of a failed state in the cohesive element, it is assumed that the cohesive element in the TC is completely failed when the energy dissipated within the element (per unit area) is equal to 95% of the fracture energy of the TC. For the cohesive elements in the healing particles, an element is assumed to be failed (or the crack is said to be formed) when the dissipated energy in the element is equal to 10% of the fracture energy of the healing particles.

The results of the simulations are reported in terms of crack initiation temperature. In order to have a mesh-independent definition of crack initiation, a study was performed

whereby the crack is said to be formed or initiated in terms of a predefined crack length (sum of the length of the failed cohesive elements). Three different crack lengths are considered for this purpose given by 1, 2 and 3 μm. It was observed that the choice of the above crack lengths did not have a significant influence on the crack initiation temperature (error being less than 5%). To this end, the crack initiation temperature is assumed to be reached when the cumulative crack length reaches a value of 3 μm.

3.1. Effect of CTE mismatch

For the CTE mismatch study, two different simulation setups are considered, denoted as a two-particle system and a multiple particles system. The simulation set up for the two-particle system is shown in Fig. 2. The objective is to first study the effect of the CTE mismatch on the local crack evolution in the presence of two idealised healing particles whose topology/distribution is fully defined by the inter-particle distance and the orientation. Subsequently, the second setup containing a more realistic random distribution of multiple particles are modelled in the TC layer, and the crack evolution is investigated. Finally, the results obtained from the two simulation setups are compared in order to provide an explanation of failure in the multiple-systems setup based on the two-particle set up.

3.1.1. Two-particle simulation setup

Two healing particles each of radius R_P=7.5 μm are dispersed in the TC layer. The interparticle distance and the orientation between the particles are varied to study the effect of these topological/spatial parameters on the crack pattern. Five different values are assigned for the interparticle distance given by $D_P/R_P = 0.25$, 0.5, 1, 1.5 and 2, where D_P/R_P is the ratio of the normal distance between the edges of the particles to the radius of the particle. The orientation characterised by the angle θ between the line connecting the centre of the particles and the positive x-axis is assigned four values given by $\theta = 0^0, 30^0, 60^0$ and 90^0.

Two different CTE mismatch ratios, given by $\alpha_P/\alpha_{TC} = 1.5$ and 0.5 are considered for the simulations. The stress fields in and around two adjacent particles are shown in Fig. 3 at $T = 30^0$C for $D_P/R_P = 0.5$ and $\theta = 30^0$. As shown in Fig. 3a, the crack initiates between the particles when $\alpha_P/\alpha_{TC} = 1.5$ and subsequently appears on the top and the bottom of the particles (as observed with respect to the TGO interface). In contrast, the crack initiates in the periphery of the particles (i.e., "outside") when $\alpha_P/\alpha_{TC} = 0.5$ as may be observed in Fig. 3b. This example illustrates that the nucleation of cracks depends strongly on the CTE mismatch. The results of all the cases considered are summarised in Fig. 4 in terms of the crack initiation temperature in the TC layer as a function of the topological/spatial parameters. From the figure corresponding to $\alpha_P/\alpha_{TC} = 1.5$, it can be observed that the spatial parameters have, in general, a considerable influence on the crack initiation temperature. In particular, the interparticle orientation has a more significant influence on the crack initiation temperature than the interparticle distance. The crack initiation occurs earlier in the case when the particle is located one below the other as opposed to the case where they are located side by side. The following explanation holds for such observation. For the considered thermal mismatch and the loading condition (cooling),

when the particles are located one below the other, given by $\theta = 90^0$, tensile stresses are generated on the top and the bottom interface regions of both the particles. This, in turn, leads to further amplification of the driving force for the crack initiation and evolution due to the interaction between the stress fields associated with each particle. On the other hand, when $\theta = 0^0$, such tensile-tensile stress field interaction does not occur, rather a compressive-compressive stress field interaction results from such a spatial positioning of the particles. Thus, naturally, for the considered thermal mismatch ratio, the temperature drop (during the cooling process) required for crack initiation increases as the angle between the particles is decreased from 90 to 0 degrees. In terms of the interparticle distance, as highlighted

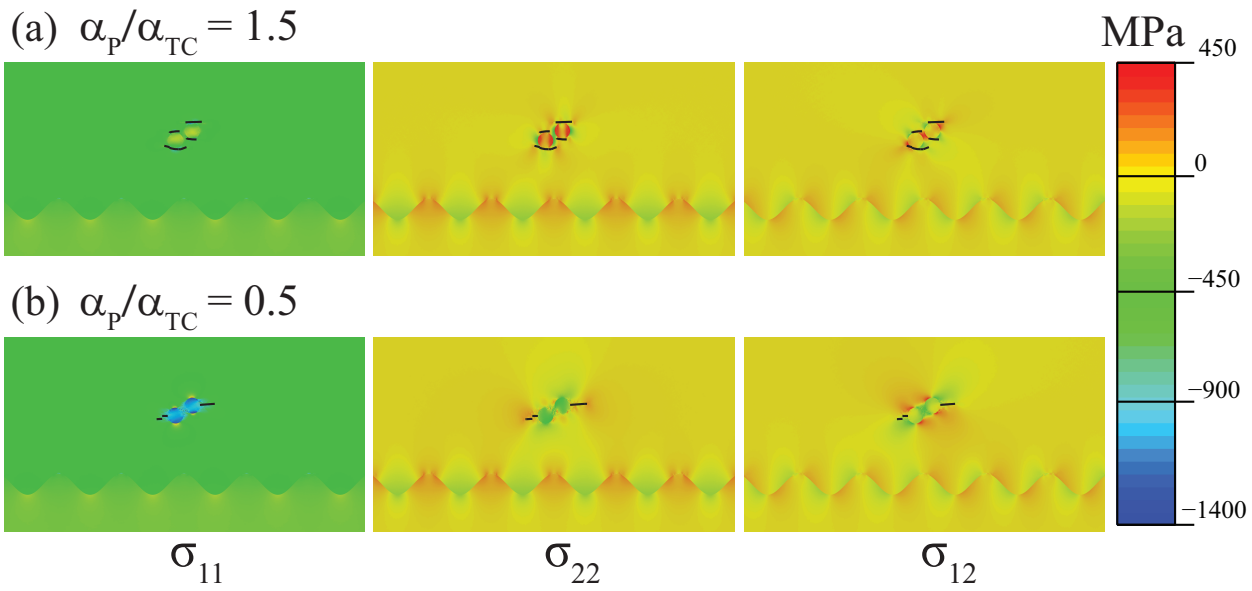

Figure 3: Stress distribution at T = 30^0C with $D_P/R_P = 0.5$ and $\theta = 30^0$ for two different CTE mismatch ratios: (a) $\alpha_P/\alpha_{TC} = 1.5$ and (b) $\alpha_P/\alpha_{TC} = 0.5$.

above, the influence is rather less than that of the orientation as can be observed from Fig. 4. For the orientations, $\theta = 60^0$ and 90^0 there is a general tendency that the crack initiation is delayed as the interparticle distance is increased. On the other hand, for $\theta = 30^0$ and 0^0, the trend is not monotonic, and it can be said that the interparticle distance does not play an influencing role on the crack evolution on an average sense.

The results corresponding to the case of the thermal mismatch ratio $\alpha_P/\alpha_{TC} = 0.5$ are shown in Fig. 4, where the thermal expansion coefficient of the particle is lower than that of the TC matrix. In this case, the trend is in general reversed as compared to the previous case albeit with a distinct behaviour observed until the interparticle distance reaches a value of 1. When the interparticle distance reaches the value equal to 1, the temperature drop required for the crack initiation is significantly larger. The trend in the variation of the crack initiation temperature is not monotonic, which can be attributed to the following observation of crack patterns: Until the interparticle distance reaches the value of 1, the microcracks are initiated in a region outside of the particle pair, whereas when the interparticle distance is

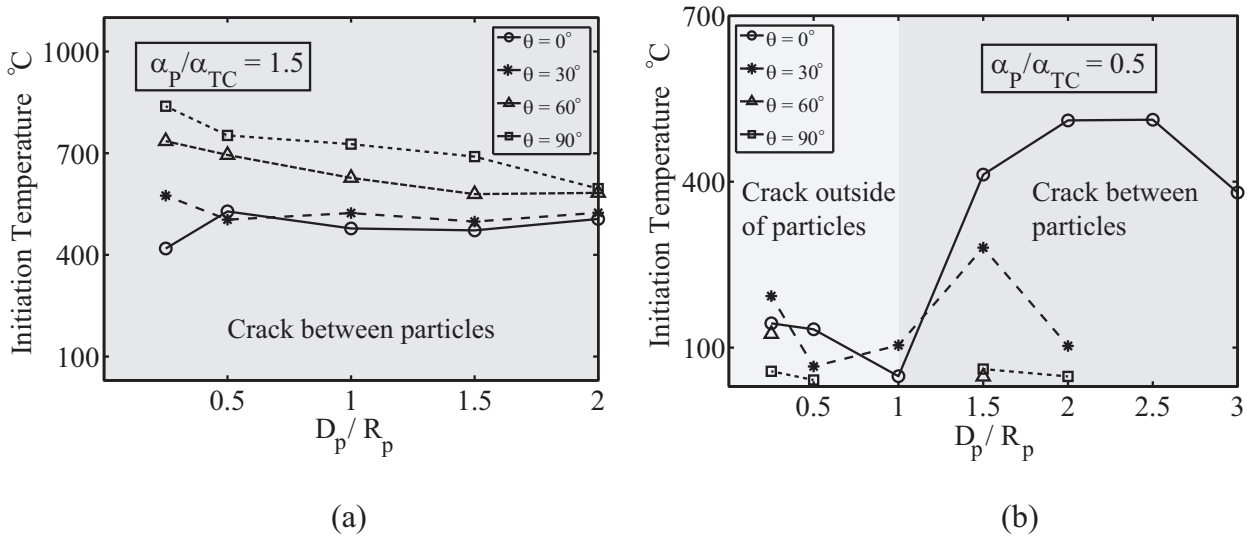

Figure 4: Crack initiation temperature vs interparticle distance for different particle orientations and for two different CTE mismatch ratios: (a) $\alpha_P/\alpha_{TC} = 1.5$ and (b) $\alpha_P/\alpha_{TC} = 0.5$. For $\alpha_P/\alpha_{TC} = 0.5$, the two shaded regions marks the location of crack initiation. In the dark grey region ($D_P/R_P > 1$) the cracks are initiated between the particles while in the light grey region ($D_P/R_P < 1$) the cracks are initiated outside of the particles.

increased beyond the value of 1, cracking occurs in the region between the two particles.

3.1.2. Multiple particles simulation setup

In this subsection, the results for the second simulation set up where a random distribution of healing particles is considered are presented. The volume fraction of the $MoSi_2$ particles is approximately 15% chosen in accordance with the self-healing TBC systems considered in [8, 29]. All healing particles have the same radius R_P=7.5 μm as used in the two-particle simulation set up. To evaluate the effect of the thermal mismatch parameter, five different values are considered in the analysis given by α_P/α_{TC} = 1.5, 1.25, 1, 0.75 and 0.5. The results of the simulations are reported in terms of the fracture pattern as shown in Fig. 5. Upon observing the cracking patterns, it can be inferred that the thermal mismatch ratio has a significant influence on the crack initiation and evolution. In particular, the fracture patterns are distinctly different for different mismatch values. In general, for a mismatch ratio larger than 1, microcracks initiate at the top and bottom edges of the healing particles, whereas for mismatch ratios lower than one, the tendency is that the cracking occurs at the left and right sides of the particles. As expected, no cracking is observed for the mismatch ratio equal to 1, i.e., the particle and the TC layer having identical values of thermal expansion coefficients. Any deviation from this value generates thermal mismatch stresses, which in turn leads to crack initiation, the severity of which depends upon the magnitude of the CTE mismatch. One interesting observation is that for the case of α_P/α_{TC} = 0.75, micro-cracks are also initiated near the TC/BC interface as observed from the figure, revealing the complex effect that the CTE mismatch has on the failure behaviour of the TBC systems. Further detailed quantification in terms of the crack initiation temperature and

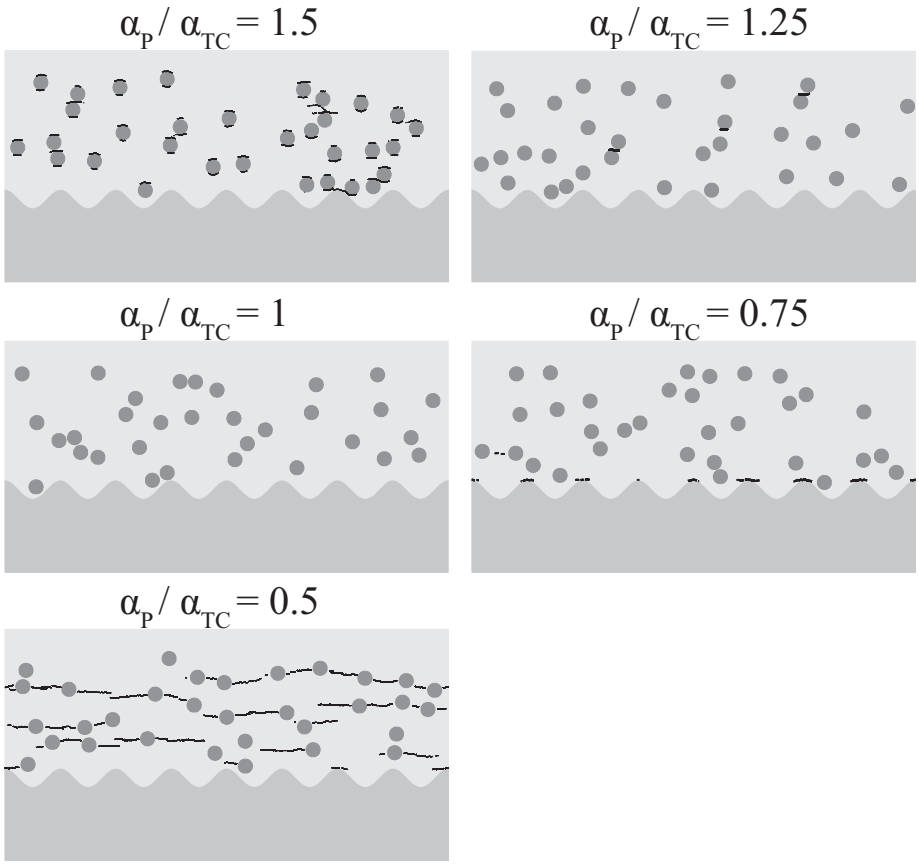

Figure 5: Self-healing TBC system showing the degree of microcracking for various CTE mismatch ratios.

total crack length can reveal the fracture characteristics in the TBC as a function of CTE mismatch. The results of such quantification are summarized in Fig. 6 whereby the crack initiation temperature and the total crack length are plotted against the thermal mismatch ratio.

As discussed before, five realisations are considered for each case of thermal mismatch ratio. Hence an average value is plotted along with the discrete standard deviations. The crack initiation occurs earlier in the TC layer with the increase or decrease in the CTE mismatch ratio from the value of 1 as shown in Fig. 6. The crack intiation behavior due to the CTE mismatch is qualitatively similar to the reported trend [45] quantified through a nondimensional mismatch parameter in ceramic composites. From the total crack length vs CTE mismatch plot, it can observed that for the case of thermal mismatch ratio of α_P/α_{TC} = 0.5, the matrix failed completely, which is attributed to the fact that the crack initiates on the left and right edges of each particle, making it far easier to grow further. In other words, once the microcracks are formed on the left and right edges of each healing particle, the stress fields associated with the microcracks corresponding to each particle synergistically interacts with the stress fields of the neighbouring microcracks (of the neighbouring particle). This, in turn, results in the interaction and further amplification of the stress fields and thus

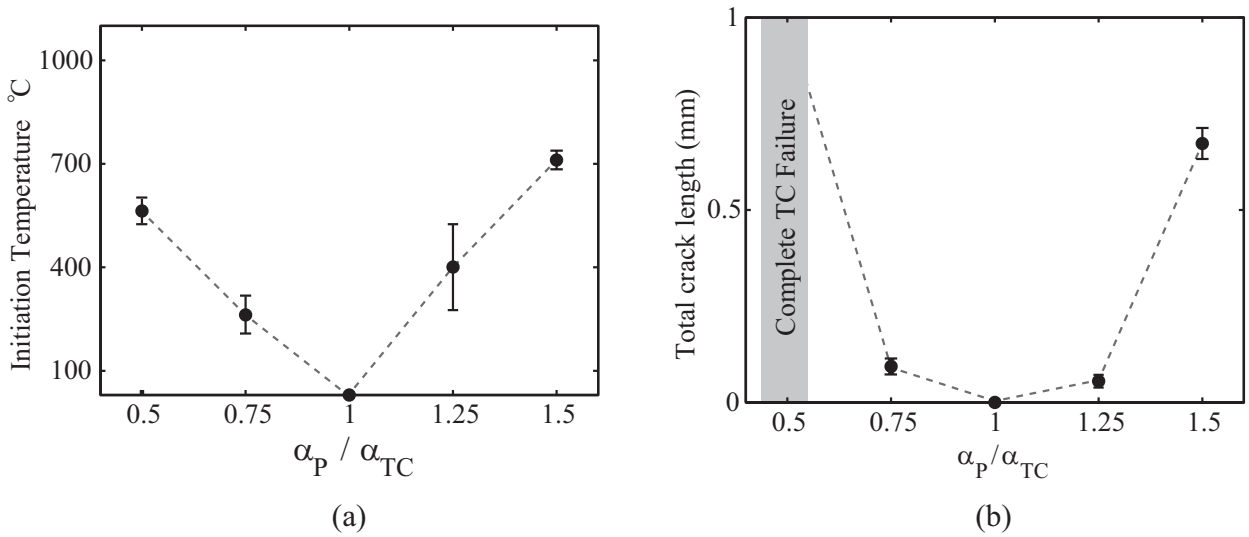

Figure 6: Variation of (a) crack initiation temperature and (b) total crack length for different CTE mismatch ratios α_P/α_{TC} = 1.5, 1.25, 1, 0.75 and 0.5. For the CTE mismatch ratio of 0.5, there is a complete failure of the TC before reaching the final temperature (30^{o}C) as indicated by a grey shade.

ultimately resulting in failure of the matrix. On the other hand, for the mismatch ratio α_P/α_{TC} = 1.5, such interactions do not occur due to the crack initiation locations, thus resulting in a relatively lower total crack length. It is generally observed that any CTE mismatch between the particles and the matrix would lead to thermal stresses and in turn result in possible microcracking, thus potentially weakening the self-healing material. In the research on extrinsic self-healing ceramics reported in [46, 47], the CTE mismatch between the healing particles and the ceramic matrix is considered as one of the important criteria for the selection of the healing agent. In contrast, for metal matrix particulate composites [48, 49] the CTE mismatch between the particle and the metal matrix is found to improve the strength and toughness of the composite material owing to the induced plastic deformation of the matrix.

3.2. Model Integration

In this subsection, a correlation is made between the results obtained from the random distribution of multiple particles with the two-particle case. The crack initiation temperature is used for the correlation using the results corresponding to two thermal mismatch coefficients namely α_P/α_{TC} equal to 0.5 and 1.5. In the TBC system with a random particle distribution, the spatial metrics of the particles are quantified in terms of the distance and the orientation between the adjacent pair of particles, which is then used to correlate with the two-particle TBC case. The results of the comparison are shown in Fig. 7, in which the crack initiation temperature is plotted for both TBC configurations as a function of the spatial metrics. The results corresponding to the two-particle case are plotted as lines and those of the multiple particle cases are plotted as dark dots superimposed onto the two-particle plots. From the results, it can be observed that the two-particle case correlates

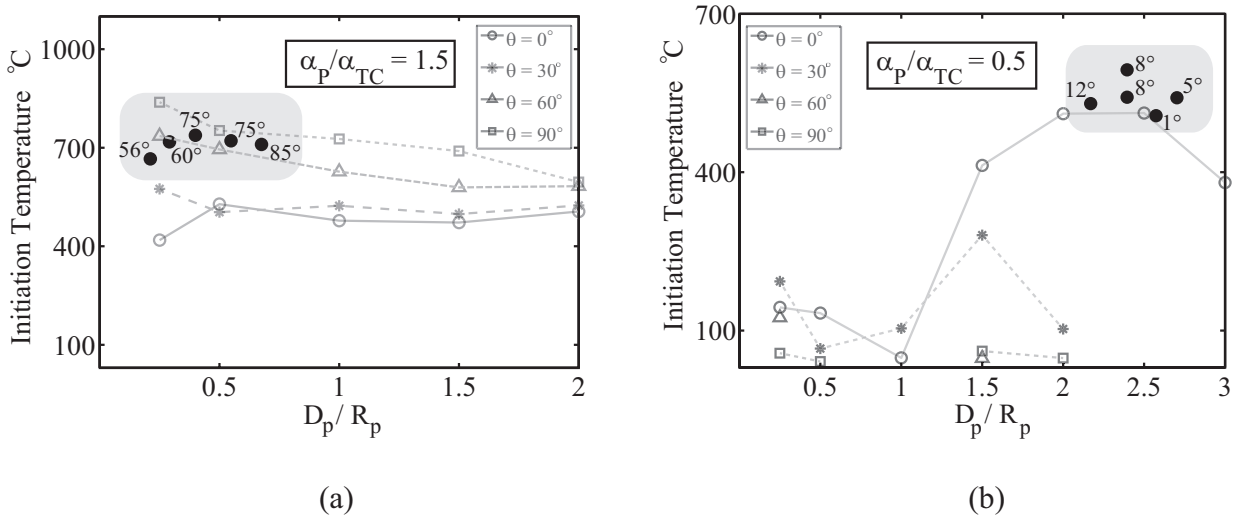

Figure 7: Correlation of crack initiation temperature of multiparticle simulation with two particle simulation case for $\alpha_P/\alpha_{TC} = 0.5$ and 1.5. This figure is analogous to Fig. 4, but the new data points marks the crack intiation temperature of multiparticle simulations (five different realisations) along with the angular dependence.

very well with the results corresponding to the TBC system with a random distribution of multiple particles. For instance, in Fig. 7 corresponding to the case of $\alpha_P/\alpha_{TC} = 1.5$, the crack initiation occurs in the vicinity of the particles whose normalised interparticle distance is between 0 and 1 and the angular orientation is between 60 to 90 degrees. In the other case for a lower thermal expansion coefficient for the particles, the crack initiation occurs in the vicinity of the particles whose interparticle distance is between 2 and 3 and the orientation is between 0 and 15 degrees. In both cases, the results from the two-particle and multiple particle cases correlate well. This indicates that a two-particle simulation is sufficient to study the interaction between the healing particles and the TBC layers in terms of crack initiation characteristics.

3.3. Effect of particle strength

The second material parameter considered in this study is the effect of the relative fracture strength of the particle with respect to the TC layer, defined by the ratio (σ_P/σ_{TC}). To investigate the effect of the strength mismatch parameter, analyses are conducted for three different values of particle strength ratio, 0.5, 1 and 3. Two subsets of analyses are conducted, one with varying the ratio of normal (tensile) strength of the particle relative to the TC matrix by keeping the shear strength ratio fixed and equal to 1. In the second subset, the ratio of the shear strength of the particle to that of the TC matrix is varied, while the normal strength ratio is kept equal to 1. Two CTE mismatch ratios $\alpha_P/\alpha_{TC} = 0.5$ and 1.5 are considered. The resulting fracture patterns obtained from the simulations are reported in Fig. 8.

The results corresponding to the thermal mismatch, $\alpha_P/\alpha_{TC} = 1.5$ is shown in the upper part of the figure. From the results, it is evident that the shear strength ratio has

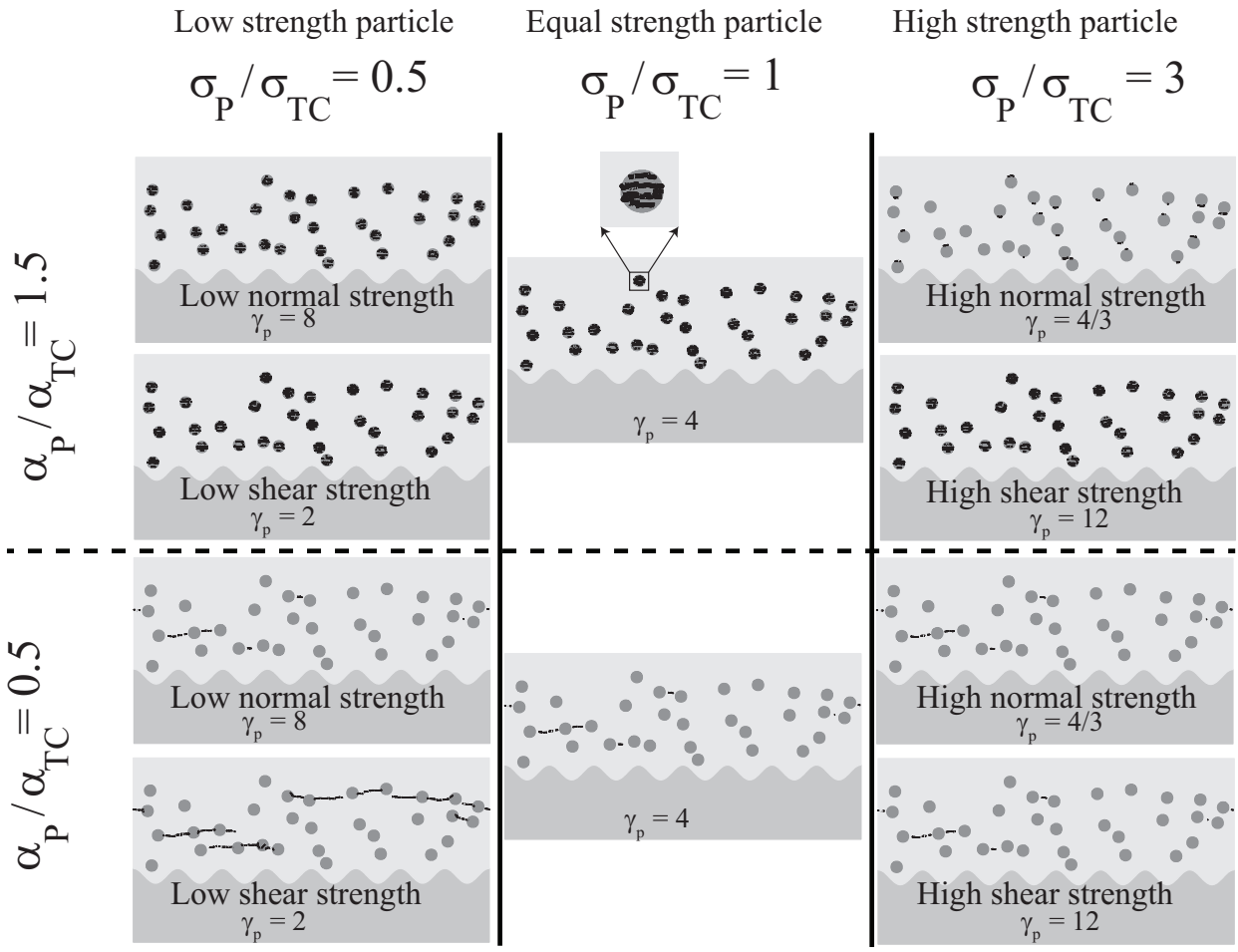

Figure 8: Fracture pattern corresponding to different particle strengths and two CTE mismatch ratios, $\alpha_P/\alpha_{TC} = 0.5$ and 1.5. In this figure, low or high normal strength corresponds to the variation of particle normal strength for a fixed shear strength ratio of 1 and vice-versa. For $\alpha_P/\alpha_{TC} = 1.5$ and the normal strength ratio (σ_P/σ_{TC}) <=1, the particle shattering is observed with multiple micro-cracks inside the particle. For $\alpha_P/\alpha_{TC} = 0.5$, complete failure of the TBC occurs. The fracture pattern for this case is shown at T = 450^{o}C which shows particle fracture before the complete failure of the TBC.

no influence on the fracture pattern, whereas the ratio of the normal strength affects the fracture pattern noticeably. This is due to the fact that for the chosen thermal mismatch, tensile stresses are generated within the particles, making the particle cracking prone to tensile fracture properties, rather than shear. In the case of tensile strength ratio, distinct fracture mechanisms are observed when comparing the crack patterns for the normal strength ratios, 0.5 and 3. In particular, particle shattering occurs when the normal strength ratio is less than or equal to 1. The same type of failure mode (particle shattering) is also reported experimentally in [50] when the particles in a metallic matrix are subjected to tensile stresses. In the present case, the cracks in the particles do not grow into the TC matrix owing to the compressive stress fields in the TC layer under cooling. On the other hand, for the normal strength ratio of 3, microcracks form in the TC layer close to the top and bottom proximities

of the particles but leave the particles uncracked. In the case of the shear strength ratio, as explained above, no influence is observed, leaving similar fracture patterns for all the three cases given by shear strength ratio = 0.5, 1 and 3.

The fracture patterns corresponding to the thermal mismatch ratio equal to 0.5 are shown in the lower part of Fig. 8. One important difference between the results corresponding to the CTE mismatch 0.5 and 1.5 is that complete failure of the TBC occurs when the CTE mismatch is equal to 0.5. This can be attributed to the fact the stress field in the TC layer adjacent to the particles (to the left and the right) is tensile in nature leading to microcrack initiation in the vicinity of the particles. Further, the favourable orientations of these microcracks lead to their coalescence resulting in a large macrocrack, hence the complete failure of the TBC before reaching the room temperature. To illustrate the effect of the strength mismatch the fracture pattern shown in Fig. 8 for $\alpha_P/\alpha_{TC} = 0.5$ corresponds to the temperature 450^oC (i.e., before complete failure). Corresponding to this point of the loading history and for this CTE mismatch ratio, the role of the normal and shear strength ratios are shown in terms of the resulting fracture patterns. In principle, the influence of the strength ratios for the CTE mismatch equal to 0.5 reverses as compared with the CTE mismatch ratio equal to 1.5, see Fig. 8. Specifically, the ratio of the normal strength does not influence the fracture pattern, whereas the shear strength ratio has an effect on the fracture pattern. This is primarily because compressive stresses result in the particles due to the lower CTE of the particle with respect to the TC matrix. Thus, the shear mode of failure is dominant, and the normal stress-induced cracking is prevented due to the presence of such compressive stress field within the particles.

3.4. Effect of interface strength

The third material parameter of interest is the strength of the interface between the healing particles and the matrix. For instance, the numerical study presented in [51] reveals the influence of thermomechanical stresses induced by the CTE mismatch on interface failure of the particulate composite. In the present study, the effect of variation of the interface strength with respect to the strength of TC layer ($\sigma_{i_{P/TC}}/\sigma_{TC}$) on the fracture pattern of the TBC is considered. To explore this effect, again two subsets of simulations are carried out for the two sets of CTE mismatch values, $\alpha_P/\alpha_{TC} = 1.5$ and 0.5 as conducted in the particle strength case. In the first subset, the interface normal strength is varied for a fixed interface shear strength ratio equal to 1. In the second case, the interface shear strength is varied by fixing the interface normal strength with a value equal to 1. The results of the simulations for the different interface strength ratios, $\sigma_{i_{P/TC}}/\sigma_{TC} = 0.5$, 1 and 3 are shown in Fig. 9. The figure resembles to Fig. 8 to a high degree for the CTE mismatch ratio of 0.5 but instead of particle cracking, interface debonding is observed.

The fracture patterns corresponding to the CTE mismatch, $\alpha_P/\alpha_{TC} = 1.5$ are summarized in the upper part of the figure for various normal and shear strength ratios. From the results, it can be observed that the normal strength ratio has a noticeable influence on the fracture pattern, whereas the shear strength ratio does not affect the fracture pattern as can be seen from the figure. This is again due to the effect of tensile stress fields in and around the particles for the considered thermal mismatch. Such an effect of the normal

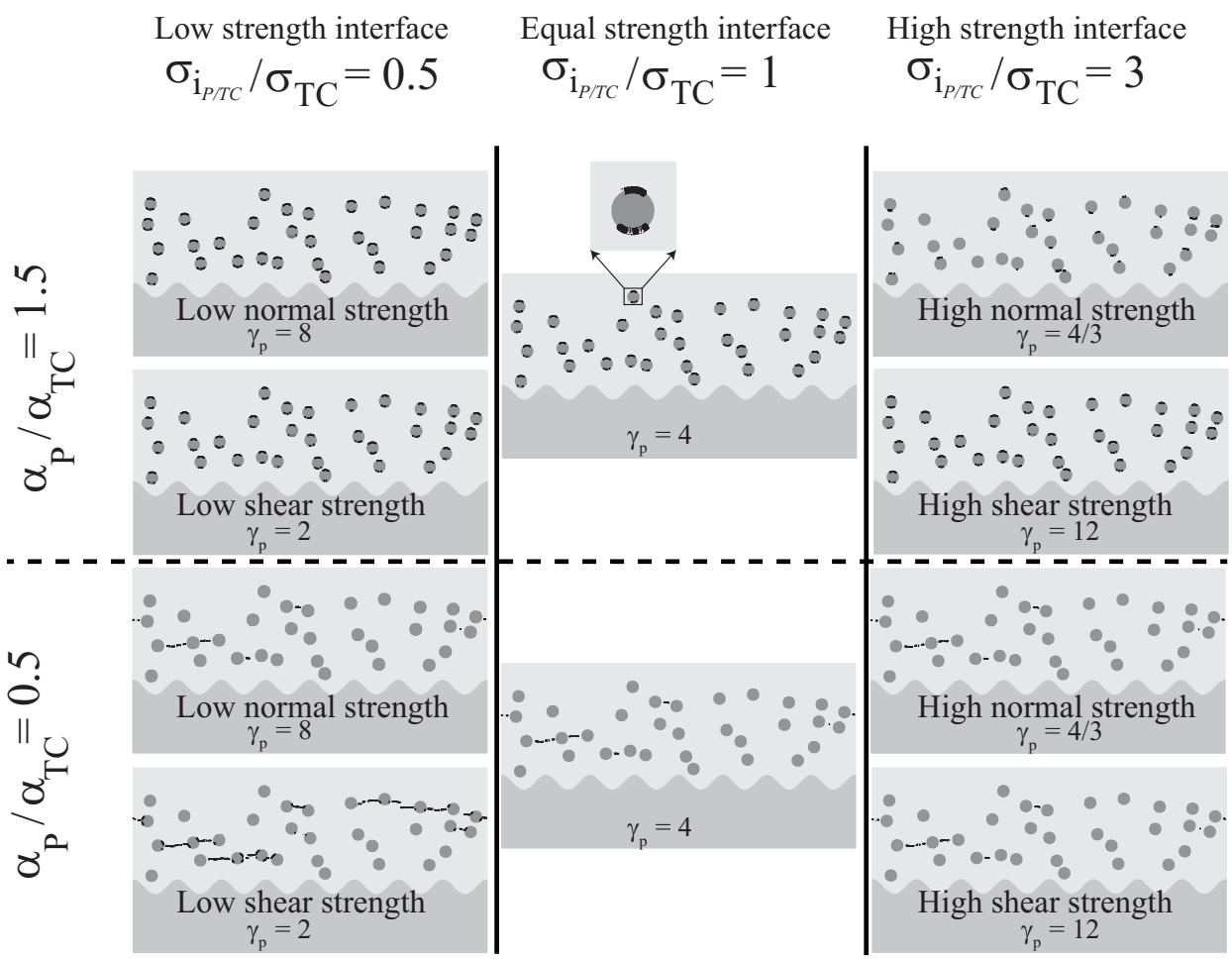

Figure 9: Fracture pattern corresponding to different interface strengths and two CTE mismatch ratios $\alpha_P/\alpha_{TC} = 0.5$ and 1.5. In this figure, low or high normal strength corresponds to the variation of interface normal strength for a fixed interface shear strength ratio of 1 and vice-versa. For $\alpha_P/\alpha_{TC} = 1.5$ and the normal strength ratio $(\sigma_{i_{P/TC}}/\sigma_{TC})$ <=1, the interface debonding occurs at the top and bottom sides of the particles. For $\alpha_P/\alpha_{TC} = 0.5$, complete failure of the TBC occurs. The fracture pattern for this case is shown at at T = 450°C which shows interface debonding between the particle and the TC before the complete failure.

strength is visible from the fracture pattern corresponding to the higher and the lower values of the normal strength ratios, in which the interface debonding becomes less severe when the normal strength ratio of the interface is increased to the value 3. The fracture patterns corresponding to the variation in the shear strength ratios are not altered.

For the CTE mismatch, $\alpha_P/\alpha_{TC} = 0.5$, the fracture patterns are shown in the bottom portion of Fig. 9. It is worth mentioning that for this CTE mismatch case, complete failure of the TBC occurs, as was the case in the particle strength study. Nonetheless, to reveal the effect of the interface strength mismatch, the fracture patterns before the complete failure are reported, i.e., at a temperature 450^{o}C. Upon comparison of the fracture patterns for the two CTE mismatch values, the effects of the normal and the shear strength ratios

are reversed. A similar observation was made in the particle strength study. The resulting fracture patterns reveal that changes in normal strength ratio of the interface do not influence the fracture pattern. On the other hand, a decrease in the shear strength leads to more microcracks resulting from the interface debonding, as in the particle strength study. The primary difference between the particle strength and the interface strength studies is that the interface debonding occurs in a stress field which is severely inhomogeneous along the interface, whereas the stress field within the particle (whether tensile or compressive) is largely homogeneous until crack initiation sets in.

In general, a weak interface can degrade the TBC mechanical properties, but would possibly offer the potential of exposing the TBC microcracks to the healing agent contained within the particle.

4. Conclusions

Finite element simulations of fracture evolution in TBC systems with embedded solid healing particles were conducted to investigate the effect of geometric and material properties of the healing particles on the crack pattern. Two different configurations of the unit-cell based TBC were analysed, one with a single pair of healing particles and the other with a random distribution of healing particles. The effects of CTE and strength mismatch between the particles and the TC layer were studied using parametric simulations. The following conclusions are drawn from the study.

- In addition to the CTE mismatch, the two-particle setup also captures the effect of topological distribution of the healing particles, characterised by the interparticle distance (D_P/R_P) and the particle orientation (θ) on the important fracture determining parameter (crack initiation temperature) quite well.

- In the two-particle case, for the higher CTE mismatch ratio ($\alpha_P/\alpha_{TC} = 1.5$), the particle orientation has a more significant effect on the crack initiation temperature than the interparticle distance whereas for the lower CTE mismatch ratio ($\alpha_P/\alpha_{TC} = 0.5$), both the orientation and the interparticle distance has a substantial effect on the crack initiation temperature.

- From the results of the multiple-particle simulations, it can be inferred that introducing the healing particles in a TBC can significantly alter the fracture pattern as compared to that of a conventional TBC system. The resulting fracture pattern is strongly determined by the CTE mismatch between the healing particles and the TC layer. In the present study, significant cracking is induced when $\alpha_P/\alpha_{TC} > 1.25$ or $\alpha_P/\alpha_{TC} < 0.75$. It is worth mentioning that for $\alpha_P/\alpha_{TC} < 1$, microcracks appear to the left and the right of the healing particles, whereas for $\alpha_P/\alpha_{TC} > 1$, the cracks appear on the top and the bottom of the healing particles.

- Very good correlations between the dual particle TBC setup and the TBC set up with a randomly distributed array of particles were observed in terms of the crack initiation temperature.

- The fracture strengths of the particle and the particle/matrix interface have a strong influence on the fracture mechanism in the TBC. Further, for the higher CTE mismatch ratio, the normal strengths of the particle and that of the interface have a prominent effect on the crack pattern as compared to the shear strengths ratios and for the lower CTE mismatch ratio, the shear strengths of the particle and that of the interface have a prominent effect on the crack pattern as compared to the normal strengths ratios.

  From the perspective of a successful self-healing TBC design, it can be suggested that $\alpha_P/\alpha_{TC} < 1$ along with lower relative fracture strength of the healing particles are desirable. Under such conditions, healing activation is favored as the observed fracture patterns reveal that the particles are open for the crack to heal in the TC layer. However, significantly lower values of α_P/α_{TC} (≤ 0.5) will lead to deterioration of the integrity of the TBC system resulting in premature failure. If the coefficient of thermal expansion of the particle is greater than the CTE of the TC ($\alpha_P/\alpha_{TC} > 1$), the simulation suggest to avoid multiple layers of particles.

Acknowledgments

This work was funded in part by the European Union's seventh framework program (FP7) through the NMP SAMBA project (grant number 309849). We extend our sincere thanks to our collaborator Prof. W.G.Sloof for his valuable support and interactive discussions.

Data Availability

The raw data required to reproduce these findings cannot be shared at this time due to technical limitations.

References

[1] T. Hille, A. Suiker, S. Turteltaub, Microcrack nucleation in thermal barrier coating systems, Engineering Fracture Mechanics 76 (6) (2009) 813–825.

[2] A. G. Evans, D. Mumm, J. Hutchinson, G. Meier, F. Pettit, Mechanisms controlling the durability of thermal barrier coatings, Progress in Materials Science 46 (5) (2001) 505–553.

[3] R. Vassen, A. Stuke, D. Stöver, Recent developments in the field of thermal barrier coatings, Journal of Thermal Spray Technology 18 (2) (2009) 181–186.

[4] R. Darolia, Thermal barrier coatings technology: critical review, progress update, remaining challenges and prospects, International Materials Reviews 58 (6) (2013) 315–348.

[5] V. Kumar, B. Kandasubramanian, Processing and design methodologies for advanced and novel thermal barrier coatings for engineering applications, Particuology 27 (2016) 1–28.

[6] W. Sloof, S. Turteltaub, A. Carabat, Z. Derelioglu, S. Ponnusami, G. Song, Crack healing in yttria stabilized zirconia thermal barrier coatings, Self Healing Materials: Pioneering Research in the Netherlands (2015) 219.

[7] Z. Derelioglu, A. Carabat, G. Song, S. van der Zwaag, W. Sloof, On the use of B-alloyed $MoSi_2$ particles as crack healing agents in yttria stabilized zirconia thermal barrier coatings, Journal of the European Ceramic Society 35 (16) (2015) 4507–4511.

[8] F. Nozahic, C. Estournès, A. L. Carabat, W. G. Sloof, S. van der Zwaag, D. Monceau, Self-healing thermal barrier coating systems fabricated by spark plasma sintering, Materials & Design 143 (2018) 204–213.

[9] T. Ouyang, X. Fang, Y. Zhang, D. Liu, Y. Wang, S. Feng, T. Zhou, S. Cai, J. Suo, Enhancement of high temperature oxidation resistance and spallation resistance of SiC-self-healing thermal barrier coatings, Surface and Coatings Technology 286 (2016) 365–375.
[10] T. Ouyang, J. Wu, M. Yasir, T. Zhou, X. Fang, Y. Wang, D. Liu, J. Suo, Effect of TiC self-healing coatings on the cyclic oxidation resistance and lifetime of thermal barrier coatings, Journal of Alloys and Compounds 656 (2016) 992–1003.
[11] S. van der Zwaag, E. Brinkman (Eds.), Self Healing Materials: Pioneering Research in the Netherlands, IOS Press, Netherlands, 2015.
[12] F. Nozahic, D. Monceau, C. Estournès, Thermal cycling and reactivity of a $MoSi_2/ZrO_2$ composite designed for self-healing thermal barrier coatings, Materials and Design 94 (2016) 444–448.
[13] A. L. Carabat, M. J. Meijerink, J. C. Brouwer, E. M. Kelder, J. R. van Ommen, S. van der Zwaag, W. G. Sloof, Protecting the $MoSi_2$ healing particles for Thermal Barrier Coatings using a sol-gel produced Al_2O_3 coating, To be published.
[14] T. Beck, M. Białas, P. Bednarz, L. Singheiser, K. Bobzin, N. Bagcivan, D. Parkot, T. Kashko, J. Petković, B. Hallstedt, S. Nemna, J. M. Schneider, Modeling of coating process, phase changes, and damage of plasma sprayed thermal barrier coatings on ni-base superalloys, Advanced Engineering Materials 12 (3) (2010) 110–126.
[15] X. Fan, W. Jiang, J. Li, T. Suo, T. J. Wang, R. Xu, Numerical study on interfacial delamination of thermal barrier coatings with multiple separations, Surface and Coatings Technology 244 (2014) 117–122.
[16] M. Białas, P. Majerus, R. Herzog, Z. Mróz, Numerical simulation of segmentation cracking in thermal barrier coatings by means of cohesive zone elements, Materials Science and Engineering A 412 (1-2) (2005) 241–251.
[17] W. Zhu, L. Yang, J. W. Guo, Y. C. Zhou, C. Lu, Determination of interfacial adhesion energies of thermal barrier coatings by compression test combined with a cohesive zone finite element model, International Journal of Plasticity 64 (2015) 76–87.
[18] T. S. Hille, S. Turteltaub, A. S. Suiker, Oxide growth and damage evolution in thermal barrier coatings, Engineering Fracture Mechanics 78 (10) (2011) 2139–2152.
[19] X. S. Yang, J. Wan, C. Y. Dai, Y. Zhang, W. G. Mao, Y. C. Zhou, C. Lu, Finite element analysis of crack propagation and fracture mechanical properties of freestanding 8wt.% Y_2O_3-ZrO_2 coatings, Surface and Coatings Technology 223 (2013) 87–91.
[20] L. Wang, D. Li, J. Yang, F. Shao, X. Zhong, H. Zhao, K. Yang, S. Tao, Y. Wang, Modeling of thermal properties and failure of thermal barrier coatings with the use of finite element methods: a review, Journal of the European Ceramic Society 36 (6) (2016) 1313–1331.
[21] M. Bäker, P. Seiler, A guide to finite element simulations of thermal barrier coatings, Journal of Thermal Spray Technology 26 (6) (2017) 1146–1160.
[22] F. Gilabert, D. Garoz, W. van Paepegem, Macro-and micro-modeling of crack propagation in encapsulation-based self-healing materials: Application of XFEM and cohesive surface techniques, Materials & Design 130 (2017) 459–478.
[23] F. Gilabert, K. van Tittelboom, E. Tsangouri, D. van Hemelrijck, N. De Belie, W. van Paepegem, Determination of strength and debonding energy of a glass-concrete interface for encapsulation-based self-healing concrete, Cement and Concrete Composites 79 (2017) 76–93.
[24] M. S. Quayum, X. Zhuang, T. Rabczuk, Computational model generation and RVE design of self-healing concrete, Frontiers of Structural and Civil Engineering 9 (4) (2015) 383–396.
[25] W. Li, Z. Jiang, Z. Yang, H. Yu, Effective mechanical properties of self-healing cement matrices with microcapsules, Materials & Design 95 (2016) 422–430.
[26] S. Ozaki, T. Osada, W. Nakao, Finite element analysis of the damage and healing behavior of self-healing ceramic materials, International Journal of Solids and Structures 100 (2016) 307–318.
[27] F. Gilabert, D. Garoz, W. van Paepegem, Stress concentrations and bonding strength in encapsulation-based self-healing materials, Materials & Design 67 (2015) 28–41.
[28] S. A. Ponnusami, S. Turteltaub, S. van der Zwaag, Cohesive-zone modelling of crack nucleation and

propagation in particulate composites, Engineering Fracture Mechanics 149 (2015) 170–190.
[29] J. Kulczyk-Malecka, X. Zhang, J. Carr, A. L. Carabat, W. G. Sloof, S. van der Zwaag, F. Cernuschi, F. Nozahic, D. Monceau, C. Estournès, et al., Influence of embedded $MoSi_2$ particles on the high temperature thermal conductivity of SPS produced yttria-stabilised zirconia model thermal barrier coatings, Surface and Coatings Technology 308 (2016) 31–39.
[30] L. Wang, F. Shao, X. Zhong, J. Ni, K. Yang, S. Tao, Y. Wang, Tailoring of self-healing thermal barrier coatings via finite element method, Applied Surface Science 431 (2018) 60–74.
[31] S. A. Ponnusami, S. Turteltaub, X. Zhang, P. Xiao, Modelling crack propagation in particle-dispersed self-healing thermal barrier coatings, in: Self Healing Materials- Pioneering Research in The Netherlands, edited by S. van der Zwaag and E. Brinkman, IOS Press, Netherlands, 2015, pp. 229–241.
[32] S. A. Ponnusami, J. Krishnasamy, S. Turteltaub, S. van der Zwaag, A micromechanical fracture analysis to investigate the effect of healing particles on the overall mechanical response of a self-healing particulate composite, to be published.
[33] S. A. Ponnusami, J. Krishnasamy, S. Turteltaub, S. van der Zwaag, A cohesive-zone crack healing model for self-healing materials, International Journal of Solids and Structures 134 (2017) 249–263.
[34] R. Vassen, S. Giesen, D. Stöver, Lifetime of plasma-sprayed thermal barrier coatings: Comparison of numerical and experimental results, Journal of Thermal Spray Technology 18 (5-6) (2009) 835–845.
[35] R. Eriksson, S. Sjöström, H. Brodin, S. Johansson, L. Östergren, X. H. Li, TBC bond coat-top coat interface roughness: Influence on fatigue life and modelling aspects, Surface and Coatings Technology 236 (2013) 230–238.
[36] C. Geuzaine, J.-F. Remacle, Gmsh: a three-dimensional finite element mesh generator with built-in pre-and post-processing facilities, International Journal for Numerical Methods in Engineering 79 (11) (2009) 1–24.
[37] T. S. Hille, T. J. Nijdam, A. S. Suiker, S. Turteltaub, W. G. Sloof, Damage growth triggered by interface irregularities in thermal barrier coatings, Acta Materialia 57 (9) (2009) 2624–2630.
[38] J. Hutchinson, A. G. Evans, On the delamination of thermal barrier coatings in a thermal gradient, Surface and Coatings Technology 149 (2-3) (2002) 179–184.
[39] A. Rabiei, A. G. Evans, Failure mechanisms associated with the thermally grown oxide in plasma-sprayed thermal barrier coatings, Acta Materialia 48 (15) (2000) 3963–3976.
[40] A. Keyvani, M. Bahamirian, A. Kobayashi, Effect of sintering rate on the porous microstructural, mechanical and thermomechanical properties of YSZ and CSZ TBC coatings undergoing thermal cycling, Journal of Alloys and Compounds 727 (2017) 1057–1066.
[41] A. Liu, Y. Wei, Finite element analysis of anti-spallation thermal barrier coatings, Surface and Coatings Technology 165 (2) (2003) 154–162.
[42] G. Thurn, G. A. Schneider, H. A. Bahr, F. Aldinger, Toughness anisotropy and damage behavior of plasma sprayed ZrO_2 thermal barrier coatings, Surface and Coatings Technology 123 (2-3) (2000) 147–158.
[43] T. S. Hille, A. S. J. Suiker, S. Turteltaub, Microcrack nucleation in thermal barrier coating systems, Engineering Fracture Mechanics 76 (6) (2009) 813–825.
[44] D. Yi, C. Li, $MoSi_2$ - ZrO_2 composites-fabrication, microstructures and properties, Doktorsavhandlingar vid Chalmers Tekniska Hogskola 261 (1328) (1997) 89–98.
[45] T. Lu, J. Yang, Z. Suo, A. Evans, R. Hecht, R. Mehrabian, Matrix cracking in intermetallic composites caused by thermal expansion mismatch, Acta Metallurgica et Materialia 39 (8) (1991) 1883–1890.
[46] L. Boatemaa, C. Kwakernaak, S. van der Zwaag, W. G. Sloof, Selection of healing agents for autonomous healing of alumina at high temperatures, Journal of the European Ceramic Society 36 (16) (2016) 4141–4145.
[47] L. Boatemaa, J. C. Brouwer, S. van der Zwaag, W. G. Sloof, The effect of the TiC particle size on the preferred oxidation temperature for self-healing of oxide ceramic matrix materials, Journal of Materials Science 53 (8) (2018) 5973–5986.
[48] M. Taya, S. Hayashi, A. S. Kobayashi, H. S. Yoon, Toughening of a Particulate-Reinforced Ceramic-Matrix Composite by Thermal Residual Stress, Journal of the American Ceramic Society 73 (5) (1990)

1382–1391.
[49] N. Chawla, Y.-L. Shen, Mechanical Behavior of Particle Reinforced Metal Matrix Composites, Advanced Engineering Materials 3 (6) (2001) 357–370.
[50] T. Mochida, M. Taya, D. J. Lloyd, Fracture of Particles in a Particle/Metal Matrix Composite under Plastic Straining and Its Effect on the Young's Modulus of the Composite, Materials Transactions, JIM 32 (10) (1991) 931–942.
[51] Y. M. Ito, M. Rosenblatt, L. Y. Cheng, F. F. Lange, A. G. Evans, Cracking in particulate composites due to thermalmechanical stress, International Journal of Fracture 17 (5) (1991) 483–491.